

Modelling time-dependent cracking in reinforced concrete using bond-slip Interface elements

Kak Tien Chong[†], R. Ian Gilbert[‡] and Stephen J. Foster^{‡†}

*School of Civil and Environmental Engineering
The University of New South Wales, UNSW Sydney, 2052. Australia*

Abstract. A two-dimensional nonlinear finite element model is developed to simulate time-dependent cracking of reinforced concrete members under service loads. To predict localized cracking, the crack band model is employed to model individual crack opening. In conjunction with the crack band model, a bond-interface element is used to model the slip between concrete and reinforcing steel permitting large slip displacements between the concrete element nodes and the steel truss element nodes at crack openings. The time-dependent effects of concrete creep and shrinkage are incorporated into the smeared crack model as inelastic pre-strains in an iterative solution procedure. Two test examples are shown to verify the finite element model with good agreement between the model and the observed test results.

Keywords: concrete; cracking; creep; shrinkage; time; finite element.

1. Introduction

Cracking is inevitable in most reinforced concrete structures under normal in-service conditions. For a structure to remain serviceable, crack widths must be small enough to be acceptable from an aesthetic point of view and small enough to avoid waterproofing problems and to prevent the ingress of water that may lead to corrosion of the reinforcement. Crack control is therefore an important aspect of the design of reinforced concrete structures at the serviceability limit state and the topic has received much research attention. However, simplified procedures for crack control in most design codes are generally less than adequate. Code methods have been developed, in the main, from laboratory observations of the instantaneous behaviour of reinforced concrete members under load and fail to account for the time-dependent development of cracking and the inevitable increase in crack widths with time (due primarily to shrinkage).

The quality of bond between reinforcing steel and concrete has a marked influence on crack formation in reinforced concrete structures, both in terms of the spacing between cracks and the crack width. Consider a reinforced concrete member subjected to an axial tensile force, as shown in Fig. 1a. The first primary crack is formed when the concrete stress, transferred from the steel reinforcement via bond, reaches the tensile strength of the concrete. This first crack occurs at that section along the member where the tensile strength is lowest. At the crack, the concrete stress is zero, the steel carries the entire tensile force, slip takes place between the concrete and the steel and

[†] Graduate Student

[‡] Professor

^{‡†} Associate Professor

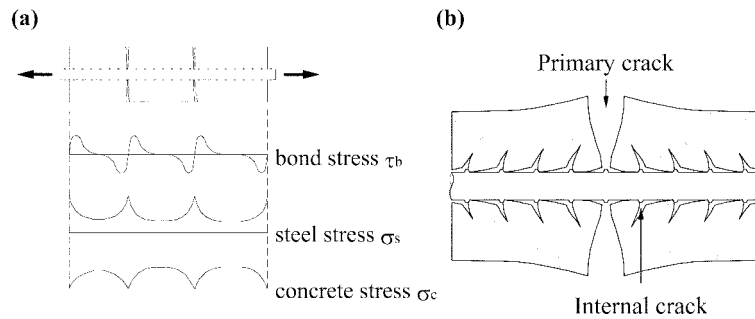


Fig. 1 Cracking in a reinforced concrete element: (a) Direct tension member and stress distributions; (b) Stress transfer by bond

the bond stress is zero. Adjacent to the crack, the bond stress τ_b initially increases, the tensile stress in the concrete σ_c increases and the tensile stress in the steel σ_s decreases. At some distance s_0 from the first crack, the bond stress reduces to zero and the concrete and steel stresses are unaffected by the crack.

If the tensile force is increased, a second primary crack will form when the concrete tensile strength is exceeded on the next weakest section at a distance greater than s_0 from the first crack. The process continues until the final crack pattern is established. No further cracking can occur if the distance between the cracks is not large enough to develop sufficient bond to allow the concrete stress on any section between the cracks to reach the concrete tensile strength. The final crack spacing is therefore somewhere between s_0 and $2s_0$. Fig. 1b shows a magnified view of the concrete-steel debonding at the primary crack.

In numerical models of cracking in reinforced concrete structures, two different approaches are commonly employed to model bond between steel and concrete. The first includes a wide range of “smeared crack models”. The inclusion of bond-slip is made possible in an indirect manner by accounting for the tensile force carried by the intact concrete between the cracks, namely tension stiffening. The tension stiffening effect has been incorporated in several different ways. One approach, developed by Scanlon and Murray (1974), is to adopt a descending branch in the concrete tensile stress-strain curve. An alternative approach proposed by Gilbert and Warner (1978) is to modify the stress-strain relationship of the tensile steel to indirectly model the tension in the concrete and to assume that the concrete possesses zero stiffness after cracking. These approaches can account for the effects of cracking at the macroscopic level of the member or structure but not at the mezzo or micro levels. Crack widths can be calculated from strains based on determined crack spacings. For example, Vecchio (1989) used the crack spacing equation proposed by Vecchio and Collins (1986) with the crack spacing given by

$$s_{rm} = \left[\frac{\sin \theta_c}{s_{rmx0}} + \frac{\cos \theta_c}{s_{rmy0}} \right]^{-1} \quad (1)$$

where s_{rmx0} and s_{rmy0} are the uniaxial crack spacings in the X- and Y-reinforcement directions, respectively, and θ_c is the angle between the crack direction and the X-reinforcement direction. Using a stepped rigid-perfectly plastic bond slip model, Marti, *et al.* (1998) derived the uniaxial

rack spacing equation

$$s_{rm0} = \frac{f_{ct}\phi(1-\rho)}{2\tau_{b0}\rho} \quad (2)$$

where f_{ct} is the concrete tensile strength, ϕ is the diameter of the reinforcing bars, τ_{b0} is the plastic bond strength and ρ is the reinforcement ratio. In applying Eq. (2) to the X- and Y-direction reinforcement s_{rm0} is replaced by s_{rmx0} and s_{rmy0} and ρ replaced by ρ_x and ρ_y , respectively. By taking as negligible the small elastic strains over the crack surface, crack widths (w_{cr}) are given by

$$w_{cr} = s_{rm}\epsilon_{av} \quad (3)$$

where ϵ_{av} is the average strain in the element.

The second approach for modelling bond involves the use of discrete bond elements to accommodate and simulate relative displacement between steel and concrete. These bond elements can be subdivided into two general types, the bond link element and the interface element. The former was developed by Ngo and Scordelis (1967). Bond is modelled by placing a bond link element between each individual node along the concrete-steel interface. The element consists of two orthogonal springs that transmit shear and normal tractions between the bond-slip surfaces. The second type, the interface element, was introduced by Goodman, *et al.* (1968) for modelling rock joints. Interface elements are now commonly used in modelling discrete crack propagation (Červenka 1994) as well as bond-slip phenomena in reinforced concrete structures (Mehlhorn and Keuser 1985, Rots 1985, Rots 1988) and are formulated using a continuous relative displacement field with the use of interpolation functions. Interface elements are placed continuously along the concrete-steel interface eliminating a major drawback of the bond link elements which are discretely inserted at the nodes.

In this study, a non-linear finite element model is developed that simulates the time-dependent behaviour of reinforced concrete structures at service loads. Bond-slip interface elements are utilized in conjunction with the use of a concrete fracture model and the rate of creep method for the time analysis of concrete structures. With the coupling of the bond-slip interface elements and a concrete fracture model, localized cracking of reinforced concrete can be captured at discrete locations and the time-dependent development of crack width and crack spacings can be calculated in a realistic manner. Comparisons are made between numerical calculations and experimental observations of the time-dependent development of cracking for two reinforced concrete flexural members under sustained transverse loads.

2. Finite element formulation

2.1. Concrete membrane element

The base element used in this research for the modelling of plane concrete is taken from that presented in Foster and Marti (2002, 2003). The element is a four-node element with the concrete taken as orthotropic and having a material elasticity matrix described by

$$\mathbf{D}_{c12} = \frac{1}{1 - \nu_{12}\nu_{21}} \begin{bmatrix} E_{c1} & \nu_{12}E_{c1} & 0 \\ \nu_{21}E_{c2} & E_{c2} & 0 \\ 0 & 0 & (1 - \nu_{12}\nu_{21})G_{c12} \end{bmatrix} \quad (4)$$

where ν is the Poisson's ratio of concrete; E_{c1} and E_{c2} are the concrete secant elastic moduli in the principal directions and; G_{c12} is the concrete secant shear modulus. To model the non-linear behaviour of concrete, E_{c1} , E_{c2} and G_{c12} are updated according to the state of the concrete element. For plane stress problems in a global coordinate system, stress is related to strain by

$$\boldsymbol{\sigma} = \mathbf{D}\boldsymbol{\varepsilon} \quad (5)$$

where $\boldsymbol{\sigma} = [\sigma_x \sigma_y \tau_{xy}]^T$ and $\boldsymbol{\varepsilon} = [\varepsilon_x \varepsilon_y \gamma_{xy}]^T$.

For known displacements and, hence, strains, the secant moduli is determined using the equivalent uniaxial strain concept proposed by Darwin and Pecknold (1977). This is done by removing the lateral deformation caused by the Poisson's effect and is given by Foster and Marti (2003) as

$$\begin{bmatrix} \varepsilon_{1u} \\ \varepsilon_{2u} \end{bmatrix} = \frac{1}{1 - \nu_{12}\nu_{21}} \begin{bmatrix} 1 & \nu_{12} \\ \nu_{21} & 1 \end{bmatrix} \begin{bmatrix} \varepsilon_1 \\ \varepsilon_2 \end{bmatrix} \quad (6)$$

where ε_{1u} and ε_{2u} are the equivalent uniaxial strains and ε_1 and ε_2 are the strains in the principal 1-2 directions. The secant moduli is obtained directly from the appropriate uniaxial material stress-strain curve and the biaxial stresses calculated from

$$\begin{bmatrix} \sigma_1 \\ \sigma_2 \end{bmatrix} = \begin{bmatrix} E_{c1} & 0 \\ 0 & E_{c2} \end{bmatrix} \begin{bmatrix} \varepsilon_{1u} \\ \varepsilon_{2u} \end{bmatrix} \quad (7)$$

The shear modulus is taken as that of Attard, *et al.* (1996) and is given by

$$G_{c12} = \frac{1}{4(1 - \nu_{12}\nu_{21})} [E_{c1}(1 - \nu_{12}) + E_{c2}(1 - \nu_{21})] \quad (8)$$

For cracked concrete, the Poisson's ratios are taken as zero and Eq. (4) reduces to

$$\mathbf{D}_{c12} = \begin{bmatrix} E_{c1} & 0 & 0 \\ 0 & E_{c2} & 0 \\ 0 & 0 & G_{c12} \end{bmatrix} \quad (9)$$

For the construction of the element stiffness matrix in global coordinates, the material stiffness is transformed such that

$$\mathbf{D}_c = \mathbf{T}_\boldsymbol{\varepsilon}^T \mathbf{D}_{c12} \mathbf{T}_\boldsymbol{\varepsilon} \quad (10)$$

where \mathbf{D}_c is the material matrix in the global coordinate system and $\mathbf{T}_\boldsymbol{\varepsilon}$ is the strain transformation

matrix. The element stiffness matrix is obtained by virtual work and is

$$\mathbf{K}_e = \int_V \mathbf{B}^T \mathbf{D}_c \mathbf{B} dV \quad (11)$$

where V is the volume of the concrete element and \mathbf{B} is the strain-displacement matrix for the two-dimensional plane stress element.

2.2. Bond-slip interface element

A 4-node interface element (shown in Fig. 2a) is used to model bond-slip between the reinforcing steel and the concrete. The relative displacement between node set 1 (consisting of nodes 1 and 4) and node set 2 (nodes 2 and 3) represents the slip between the concrete and the steel and is given by

$$\Delta u_{ti} = u_{ti}^+ - u_{ti}^- \quad \text{and} \quad \Delta u_{ni} = u_{ni}^+ - u_{ni}^- \quad (12)$$

where the superscripts “+” and “-” denote the upper and lower faces of the interface element, respectively, and the subscripts t and n represent shear and normal movement, respectively.

The relative nodal displacements $\Delta \mathbf{u}_i$ are linked to the continuous displacement field $\Delta \mathbf{u}$ by

$$\Delta \mathbf{u} = \sum_{i=1}^2 N_i \Delta \mathbf{u}_i = \mathbf{B} \mathbf{u}_e \quad (13)$$

where N_i ($i = 1, 2$) are linear shape functions.

The matrix \mathbf{B} in Eq. (13) relates the continuous field relative displacements to the nodal displacements along the interface and is given by

$$\mathbf{B} = \begin{bmatrix} -N_1 & 0 & -N_2 & 0 & N_2 & 0 & N_1 & 0 \\ 0 & -N_1 & 0 & -N_2 & 0 & N_2 & 0 & N_1 \end{bmatrix} \quad (14)$$

The element stiffness matrix is computed by applying the principals of virtual work and gives

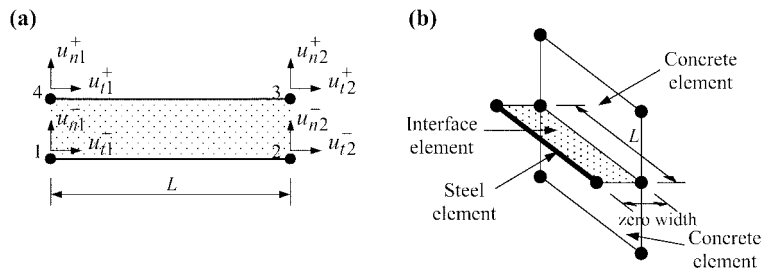


Fig. 2 Bond interface element: (a) Four-node isoparametric interface element; (b) Connectivity of interface element to concrete and steel elements

$$\mathbf{K}_e = \int_{A_e} \mathbf{B}^T \mathbf{D}_b \mathbf{B} dA \quad (15)$$

where A_e is the tangential contact surface area between the interface element and the adjacent materials and \mathbf{D}_b is the constitutive model relating the bond stress to the relative displacements between the reinforcing steel and the concrete. For the one dimensional bond formulation used in this study (see Fig. 2b), A_e is the surface area of the reinforcing bar encased in the concrete and \mathbf{D}_b is given by

$$\mathbf{D}_b = \begin{bmatrix} E_{bt} & 0 \\ 0 & E_{bn} \end{bmatrix} \quad (16)$$

where E_{bt} is the bond stress-slip modulus for the current stress state and E_{bn} is the normal bond stress-split modulus. To maintain compatibility between the reinforcing steel and the concrete in the normal direction, a stiff value for E_{bn} is used. In the tangential direction the CEB-FIP (1993) model is used to define the bond-stress versus slip relationship and is shown in Fig. 3. For stability of the solution process the bond stiffness E_{bt} is taken as the secant stiffness in a modified Newton-Raphson solution process.

For the four-node linear bond element, integration of Eq. (15) is undertaken explicitly giving

$$\mathbf{K}_e = \frac{cL}{6} \begin{bmatrix} 2E_{bt} & 0 & E_{bt} & 0 & -E_{bt} & 0 & -2E_{bt} & 0 \\ & 2E_{bn} & 0 & E_{bn} & 0 & -E_{bn} & 0 & -2E_{bn} \\ & & 2E_{bt} & 0 & -2E_{bt} & 0 & -E_{bt} & 0 \\ & & & 2E_{bn} & 0 & -2E_{bn} & 0 & -E_{bn} \\ & & & & 2E_{bt} & 0 & E_{bt} & 0 \\ & & & & & 2E_{bn} & 0 & E_{bn} \\ sym. & & & & & & 2E_{bt} & 0 \\ & & & & & & & 2E_{bn} \end{bmatrix} \quad (17)$$

where c is the sum of the bar circumferences of all bars on a layer and L is the length of the bond

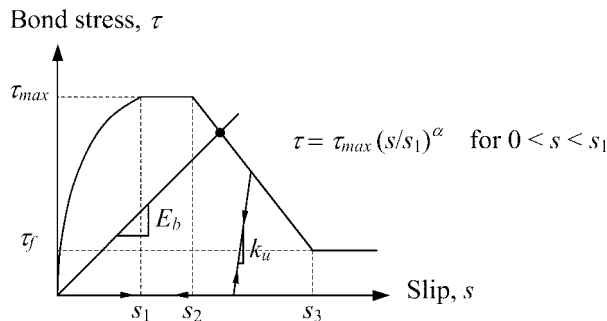


Fig. 3 Bond stress versus slip relationship (CEB-FIP 1993)

element. The bond-element stiffness matrix \mathbf{K}_b in the global coordinate system is obtained by

$$\mathbf{K}_b = \mathbf{T}_b^T \mathbf{K}_e \mathbf{T}_b \quad (18)$$

where \mathbf{T}_b is a diagonal bond-displacement transformation matrix

$$\mathbf{T}_b = [\mathbf{T}_e \mathbf{T}_e \mathbf{T}_e \mathbf{T}_e] \quad (19a)$$

$$\mathbf{T}_e = \begin{bmatrix} \cos \phi & \sin \phi \\ -\sin \phi & \cos \phi \end{bmatrix} \quad (19b)$$

where ϕ is the angle of the interface element to the global X-axis.

3. Material constitutive models

The aim of this study is to investigate the cracking behaviour of reinforced concrete members under in-service conditions. Under such conditions, the concrete in compression is rarely stressed to greater than 50 percent of its uniaxial strength and the reinforcing steel is in its elastic range. Thus, simple formulations for the concrete in compression and steel reinforcement in tension and compression are sufficient for accuracy of the numerical model. The formulations used are those presented in Foster and Marti (2003).

3.1. Fracture of concrete the crack band model

To capture the localization of concrete cracking in a smeared crack model, it is important to evaluate the strains within the fracture zones. This is complicated by the roughness and irregularity of the crack surface, the presence of microcracks, the effects of aggregate interlock and more. In this paper the crack band model of Bazant and Oh (1983) is used for concrete in tension.

With the smeared crack approach, the softening curve is expressed in the context of stress and strain and Bazant and Oh (1983) expressed the fracture energy (G_f) in the form of a fracture energy density parameter g_f where

$$g_f = G_f/h_c = \int \sigma d\varepsilon_p \quad (20)$$

where h_c is a characteristic length and represents the width of the fracture zone. The crack width w_{cr} is given by

$$w_{cr} = \varepsilon_p h_c \quad (21)$$

where ε_p is the plastic component of strain which, in-turn, is calculated by

$$\varepsilon_p = \varepsilon_1 - \varepsilon_{ce} \quad (22)$$

where ε_1 is the principal tensile strain and ε_{ce} is the elastic component of strain given by $\varepsilon_{ce} = \sigma_1/E_c$.

In this study, the bilinear tensile stress crack opening displacement model of Petersson (1981) is

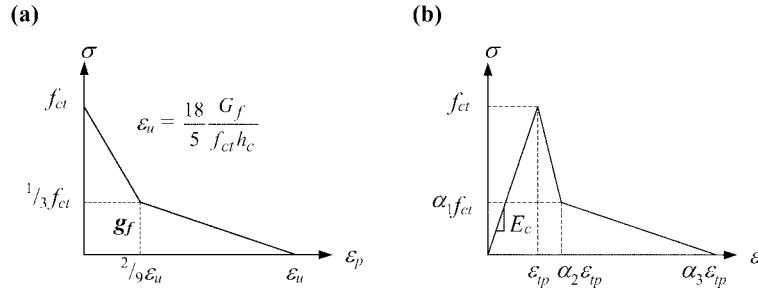


Fig. 4 Bilinear strain-softening model for concrete (Pettersson 1981): (a) Tensile stress versus plastic strain curve; (b) Tensile stress-strain curve

used. The softening branch is converted to stress-strain, as described above, and is shown in Fig. 4. Three softening parameters are used to define the curve α_1 , α_2 and α_3 , where

$$\alpha_1 = \frac{1}{3}; \quad \alpha_2 = \frac{2}{9}\alpha_3 + \alpha_1; \quad \alpha_3 = \frac{18}{5} \frac{G_f}{f_{ct} h_c \epsilon_{tp}} \quad (22)$$

3.2. Time-dependent behaviour of concrete

The major factors affecting the time-dependent behaviour of reinforced concrete structures are creep and shrinkage of the concrete. In addition, the bond stress-slip relationship changes with time and can also cause a time-dependent increase in crack width. The deterioration in the bond stress-slip relationship with time is not considered in this study.

At any time t after first loading, the vector of total strain is taken to be the sum of the vectors of instantaneous, creep and shrinkage strains. That is

$$\boldsymbol{\epsilon}(t) = \boldsymbol{\epsilon}_{ci}(t) + \boldsymbol{\epsilon}_{cp}(t) + \boldsymbol{\epsilon}_{sh}(t) \quad (23)$$

where $\boldsymbol{\epsilon}_{ci}$, $\boldsymbol{\epsilon}_{cp}$ and $\boldsymbol{\epsilon}_{sh}$ are the instantaneous, creep and shrinkage strain vectors, respectively, and $\boldsymbol{\epsilon} = [\epsilon_x \epsilon_y \gamma_{xy}]^T$. For finite element implementation, creep and shrinkage strains are treated as pre-strains updated with time and applied to the structure as equivalent nodal forces as follows

$$\mathbf{P}_0 = \int_V \mathbf{B}^T \mathbf{D}_c \boldsymbol{\epsilon}_0 dV \quad (24)$$

where \mathbf{B} and \mathbf{D}_c are as defined in Eq. (11), and $\boldsymbol{\epsilon}_0$ is the pre-strain vector which is the sum of the creep and shrinkage strains at the current time (t). The time-dependent development of creep and shrinkage are taken as

$$F(t) = At/(B+t) \quad (25)$$

where A and B are empirically fitted parameters obtained from test control data and $F(t)$ is the shrinkage strain or creep parameter at time t .

3.3. Shrinkage strain

Shrinkage is defined as the time-dependent and load independent strain resulting from the reduction in volume of concrete at constant temperature (due mainly to loss of water resulting from drying and hydration). Shrinkage is taken to be direction independent and shrinkage shear strain is taken as zero. Thus, the shrinkage strain vector is written as

$$\boldsymbol{\varepsilon}_{sh}(t_i) = [\boldsymbol{\varepsilon}_{sh}(t_i) \ \boldsymbol{\varepsilon}_{sh}(t_i) \ 0]^T \quad (26)$$

where $\boldsymbol{\varepsilon}_{sh}(t_i)$ is negative and with magnitude calculated from Eq. (25) using appropriate factors for A and B .

3.4. Creep strain

The rate of creep method (RCM) is used to model the time-dependent development of creep strain (Gilbert, 1988). The RCM requires as input a single creep versus time curve associated with the initial application of load. For all subsequent loadings, the creep versus time curve is assumed to be affine with that at first loading. That is, the rate of change of creep is assumed to be independent of the age at first loading. This, of course, is approximate and introduces some errors, particularly when the change of concrete stress with time is significant. However, the advantage is that the storage of the time-dependent stress history is not required.

For reinforced concrete structures under service load conditions, the concrete stress rarely exceeds 0.4 times the strength of the concrete. Accordingly, in this research, two assumptions are made: (i) creep is linear with respect to stress; and (ii) the time-dependent response in tension is identical to that in compression.

For the implementation of the RCM into the finite element model, time is discretized into small intervals and loads are taken to remain constant during each time increment. The creep strain at the current time is obtained by summing the increments of creep obtained from the previous time intervals, that is

$$\boldsymbol{\varepsilon}_{cp}(t) = \sum \frac{\sigma(t)}{E_c(\tau_0)} \Delta\phi \quad (27)$$

where $\Delta\phi$ is the change in creep coefficient during a particular time interval. The change of creep strain at time t is

$$\Delta\boldsymbol{\varepsilon}_{cp}(t) = \boldsymbol{\varepsilon}_{ce}(t) \Delta\phi(t) \quad (28)$$

where $\boldsymbol{\varepsilon}_{ce}(t)$ is the concrete instantaneous elastic strain at time t . For the finite element implementation, Eq. (28) is written as

$$\Delta\boldsymbol{\varepsilon}_{cp}(t_i) = \boldsymbol{\varepsilon}_{c12}(t_i) \Delta\phi(t_i) \quad (29)$$

where $\boldsymbol{\varepsilon}_{c12}(t_i)$ is the concrete principal instantaneous elastic strain vector at time t_i . Note that the change in creep coefficient is scalar.

The iterative procedure to calculate the change of creep strain between time steps at each gauss

point of each element is:

1. The concrete global instantaneous elastic strain vector $\boldsymbol{\varepsilon}_{ee}(t_i) = [\varepsilon_{cx}(t_i)\varepsilon_{cy}(t_i)\gamma_{cxy}(t_i)]^T$ as determined from the last time step is stored;
2. The instantaneous elastic strain vector in global directions is transformed through an angle θ using the strain transformation matrix, $\mathbf{T}_{\boldsymbol{\varepsilon}}$ to the elastic strain vector in principal directions giving $\boldsymbol{\varepsilon}_{c12}(t_i) = [\varepsilon_{c1}(t_i)\varepsilon_{c2}(t_i)0]^T = \mathbf{T}_{\boldsymbol{\varepsilon}}\boldsymbol{\varepsilon}_{ee}(t_i)$;
3. The change of creep strain in the current time step is calculated from Eq. (29), in which the change of creep coefficient is $\Delta\phi(t_i) = \phi(t_i) - \phi(t_{i-1})$;
4. The change of creep strain $\Delta\boldsymbol{\varepsilon}_{cp12}(t_i)$ is transformed through θ to the global directions restoring strains to the global directions;
5. The total creep strain is calculated by adding the global change of creep strain $\Delta\boldsymbol{\varepsilon}_{cp}(t_i)$ to the stored value of total creep strain from the last time step at time t_{i-1} . That is $\boldsymbol{\varepsilon}_{cp}(t_i) = \Delta\boldsymbol{\varepsilon}_{cp}(t_i) + \boldsymbol{\varepsilon}_{cp}(t_{i-1})$;
6. The current material stress state is calculated through $\boldsymbol{\sigma}(t_i) = D_c\{\boldsymbol{\varepsilon}(t_i) - \boldsymbol{\varepsilon}_0(t_i)\}$, in which the creep component is added into $\boldsymbol{\varepsilon}_0$ as per Eq. (24).
7. The equivalent nodal forces from the pre-strains (Eq. 24) are calculated and the out-of-balance force vector \mathbf{R} is determined as $\mathbf{R} = \{\mathbf{P}_e + \mathbf{P}_0 - \int_V \mathbf{B}^T \boldsymbol{\sigma} dV\}$, where \mathbf{P}_e is the external force vector applied to the structure.
8. The out-of-balance forces are applied to the mesh and the changes of displacements are determined. The process is repeated from step 2 until convergence of the norm of the displacement vector to a set tolerance (taken at 1% in this study).

The procedures described in steps 2 to 4 above are shown in Fig. 5.

4. Numerical examples

Nejadi and Gilbert (2003) undertook several series of long-term tests on reinforced concrete specimens. Both beam and slab specimens were tested under sustained loading for periods in excess

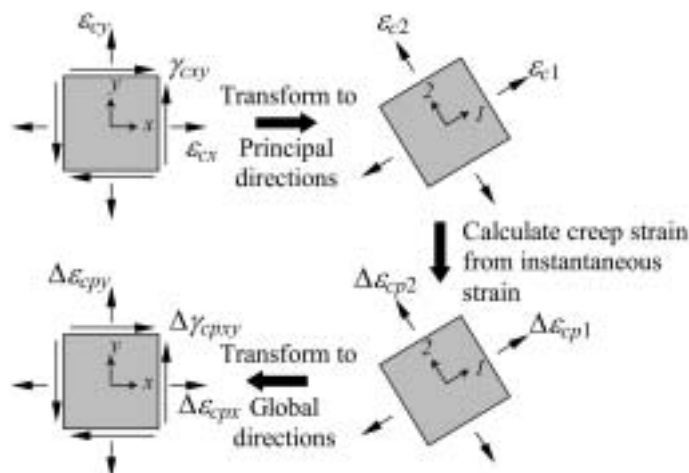


Fig. 5 Computation of creep strain from elastic strain

of 250 days to monitor the growth of flexural cracking with time. To verify the numerical model in calculating time-dependent behaviour of reinforced concrete elements, two specimens from the laboratory tests were selected and analysed using the finite element model described above. Four-node linear isoparametric elements are used for modelling the concrete, two-node bar elements for the reinforcing steel and interface elements used to model the concrete-steel bond-slip. To simulate the random cracking phenomena in real structures, stochastic fluctuations of the concrete tensile strength are introduced. In the following examples a \pm percent random fluctuation of the mean concrete tensile strength f_{ct} is assigned to the concrete elements. In the examples that follow the size of each finite element was taken as three times the maximum aggregate size as recommended by Bazant and Oh (1983).

To compare the finite element model with the experimental results, the average crack widths are calculated by summing the widths of all cracks at the soffit within the constant moment region for the beam specimen or within the region of moment greater than 90% of the maximum moment for the slab specimen. The sum of the crack widths is divided by the number of cracks within the region to give the average crack width. The crack width for the finite element model is calculated using Eq. (21) with ϵ_p a function of time. The cracked concrete element (at discrete locations) at the soffit is identified and the element crack width is calculated by averaging the crack widths computed at the gauss points of that element. The average crack width calculated in the finite element is determined in the same way as for the experimental specimens. Serviceability of a

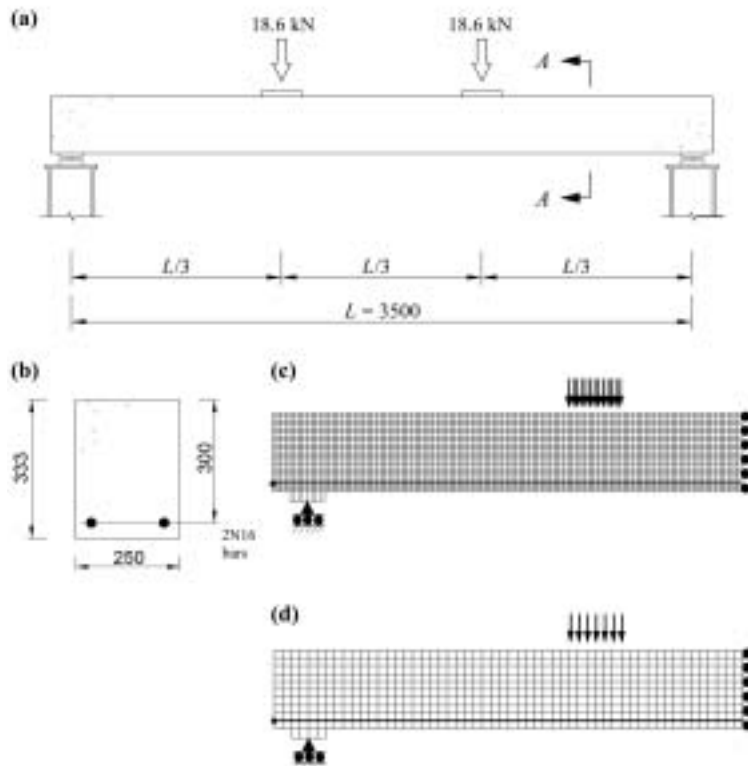


Fig. 6 Details for beam B2-a (Nejadi and Gilbert 2004): (a) Elevation; (b) Cross-section; (c) fine FE mesh; and (d) coarse FE mesh

reinforced concrete structure, however, depends not on the average crack width but on the widest crack. Therefore, the comparison of the experimental and numerical maximum crack widths is also a major interest in this study.

4.1. Example 1 : Four-point bending test under sustained load

A reinforced concrete beam, beam B2-a, tested by Nejadi and Gilbert (2004) under four-point bending and subjected to constant sustained loading is modelled. Fig. 6a shows the loading configuration and dimensions of the beam. Two FE meshes are used to model the beam; a fine mesh as shown in Fig. 6c and a coarse mesh as shown in Fig. 6d. The fine mesh consisted of 2405 nodes, 2168 concrete elements, 108 steel and 108 bond-slip elements. The coarse mesh had 665 nodes, 540 concrete elements, 54 steel elements and 54 bond-slip elements. The steel elements were connected to the concrete element via bond interface elements. The far left end node of the steel bar

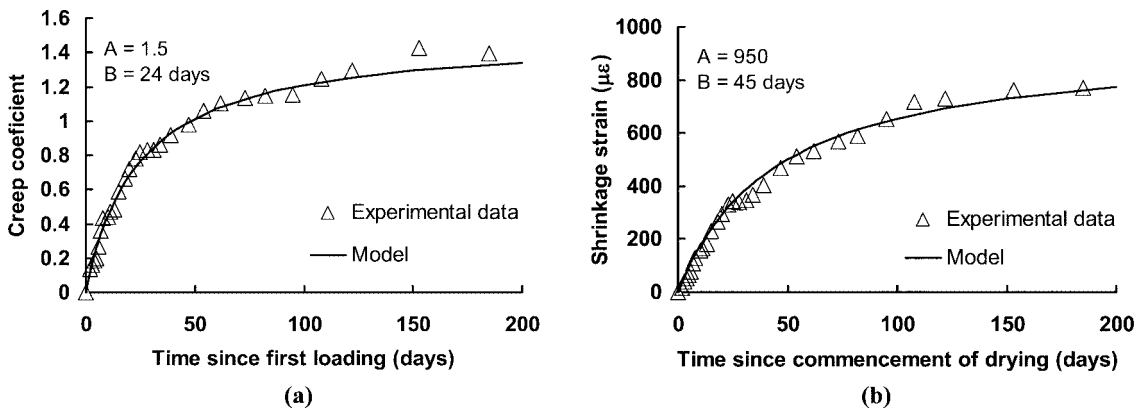


Fig. 7 Creep and shrinkage measurements of Nejadi and Gilbert (2003) compared with Eq. (28): (a) Creep coefficient versus time since first loading; (b) Shrinkage strain versus time since commencement of drying

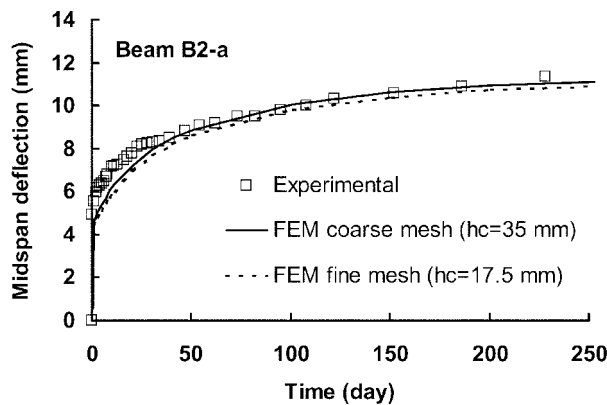


Fig. 8 Midspan deflection of beam B2-a versus time

element was rigidly connected to the concrete membrane node to simulate anchorage of the bar. The material properties for the concrete are: $f_{cm} = 25\text{MPa}$, $E_c = 25\text{GPa}$, $f_{ct} = 2.0\text{MPa}(\pm 10\%)$, $G_f = 75\text{N/m}$, $h_c = 35\text{mm}$, $\nu = 0.2$, $A_{shrinkage} = 950$, $B_{shrinkage} = 45\text{days}$, $A_{creep} = 1.5$ and $B_{creep} = 24\text{days}$. For the reinforcing steel N12 and N16 bars are 12 mm and 16 mm diameter bars, respectively, with a nominal yield strength of 500 MPa and elastic modulus of 200 GPa. The bond-slip parameters are: $s_1 = s_1 = 0.6\text{mm}$, $s_3 = 1.0\text{mm}$, $\alpha = 0.4$, $\tau_{max} = 10.0\text{MPa}$,

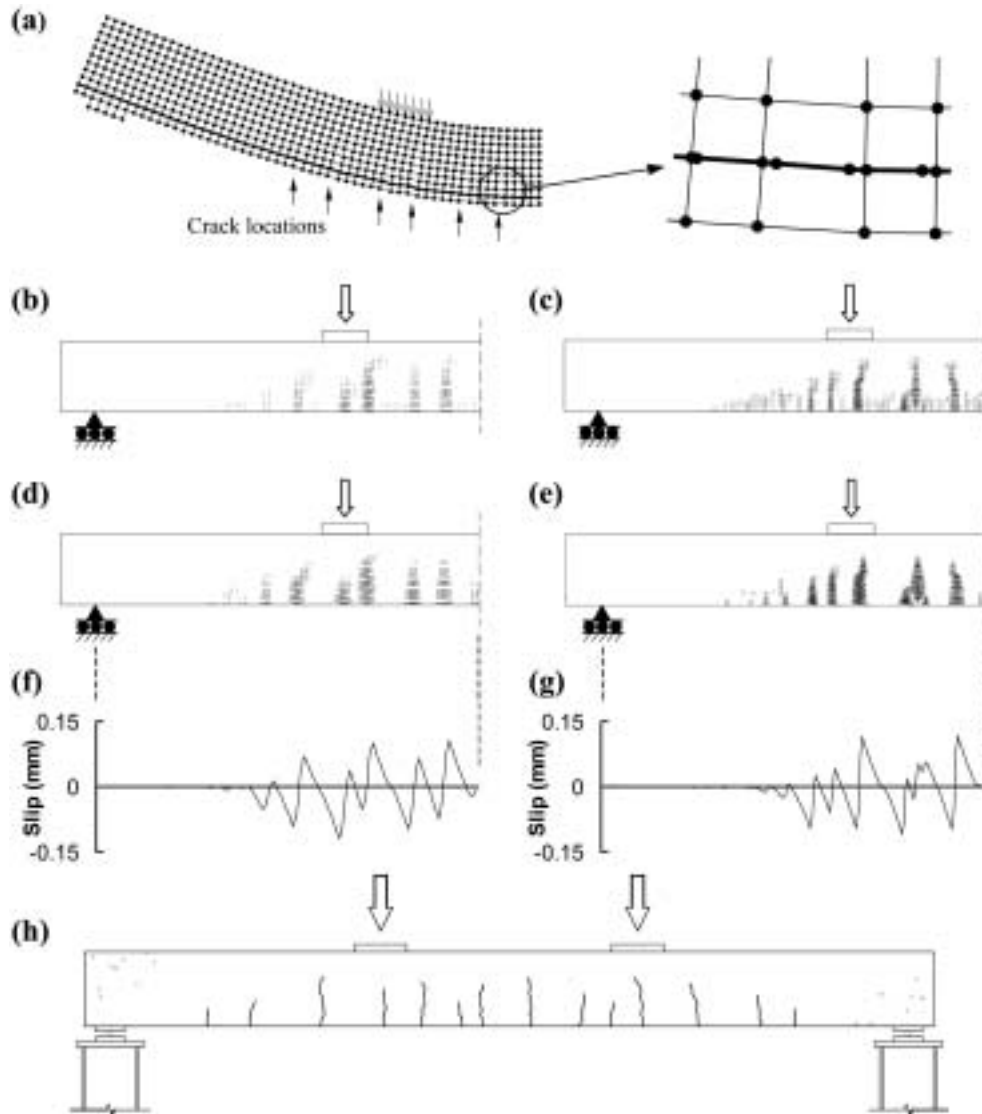


Fig. 9 Reinforced concrete beam B2-a under sustained service loads: (a) FEM deflection at 200 days (coarse mesh: scale $\times 40$) and dislocations of nodes due to bond slip at crack; (b) and (c) initial crack pattern for coarse and fine meshes, respectively; (d) and (e) crack pattern for coarse and fine meshes at 200 days, respectively (f) and (g) bond slip for coarse and fine mesh, respectively; and (h) experimentally observed final crack pattern

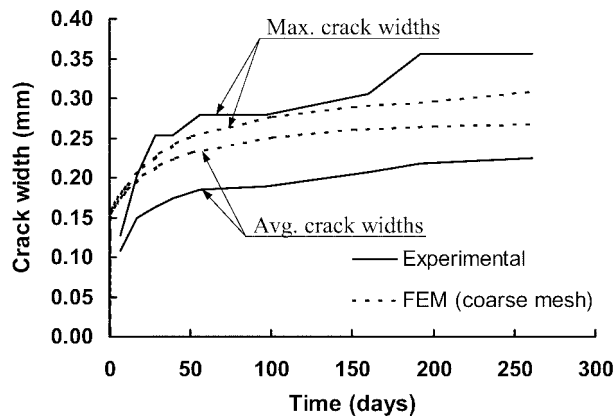


Fig. 10 Comparison of FEM and experimental crack widths with time for beam B2-a

$\tau_f = 1.5\text{MPa}$ and $k_u = 100\text{MPa/mm}$. The creep and shrinkage models given by Eq. (25) were calibrated to match the experimental control tests as shown in Figs. 7a and 7b. No correction has been made to account for size effects. Considering the cross-section dimensions of the test specimens compared to the size of the control specimens for which the shrinkage and creep relationships with time were determined, this is considered to be a reasonable supposition.

The calculated mid-span deflection versus time curve is compared with the experimental results in Fig. 8 with a good correlation for both the fine and coarse meshes. It is seen that the model is not sensitive to the mesh sizes. Figs. 9a to 9e show the crack formation with time and compare the numerical results with the experimental data (Fig. 9h) over a period of 200 days. It is shown that the computed crack spacing agrees well with the test results for both the fine and coarse meshes.

In Figs. 9f and 9g the bond-slip is plotted along the beam at time 200 days for the coarse and fine meshes, respectively. As expected, the bond-slip crosses the axis at the cracks. While the bond slips are generally small, the crack spacing and, hence, crack widths are a function of the build-up of tensile stress in the concrete, through bond with the reinforcing steel. A crack can not form closer to an existing crack than that dictated by the concrete-steel bond-slip relationship.

In the constant moment region a comparison is made in Fig. 10 between the calculated and measured crack widths at the soffit of the beam with increasing time. The comparison is presented for the change in crack width with time for the widest crack and for the average of crack width as observed in the test and as calculated by the finite element model. The agreement is reasonable, but the finite element model calculated a slightly lower maximum crack width and a higher average crack width compared to the observed results. The variation in crack widths between the FEM and the experimental data is attributed to uncertainties in the bond stress-slip relationship.

4.2. Example 2 : Uniformly loaded one-way slab under sustained load

The reinforced concrete slab S2-a tested by Nejadi and Gilbert (2003) is analysed using the FE model developed above. The slab was 163 mm thick, spanned 3.5 metres and had a total uniform load of 4.86 kN/m (excluding self weight). Details of the slab are shown in Figs. 11a and 11b. The

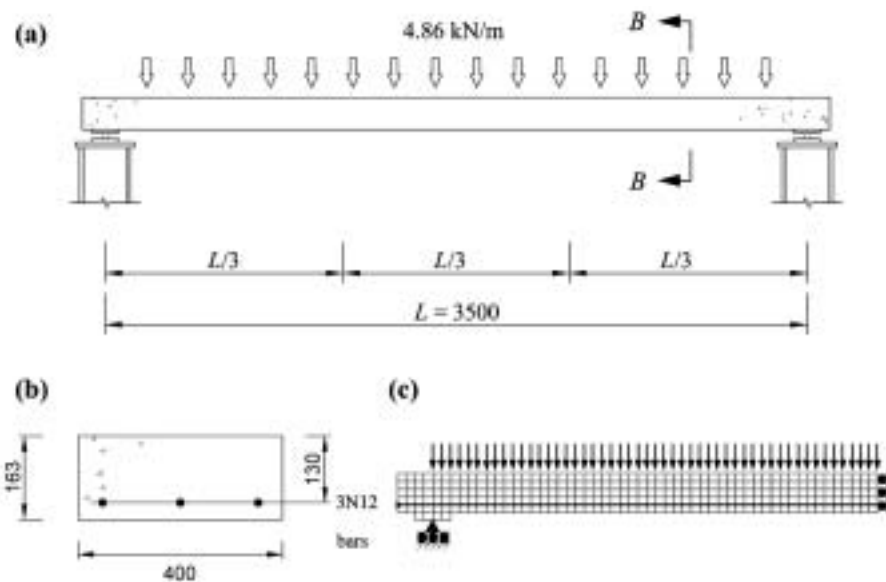


Fig. 11 Details for Nejadi and Gilbert (2004) slab S2-a: (a) Elevation; (b) Cross-section; (c) Finite element mesh

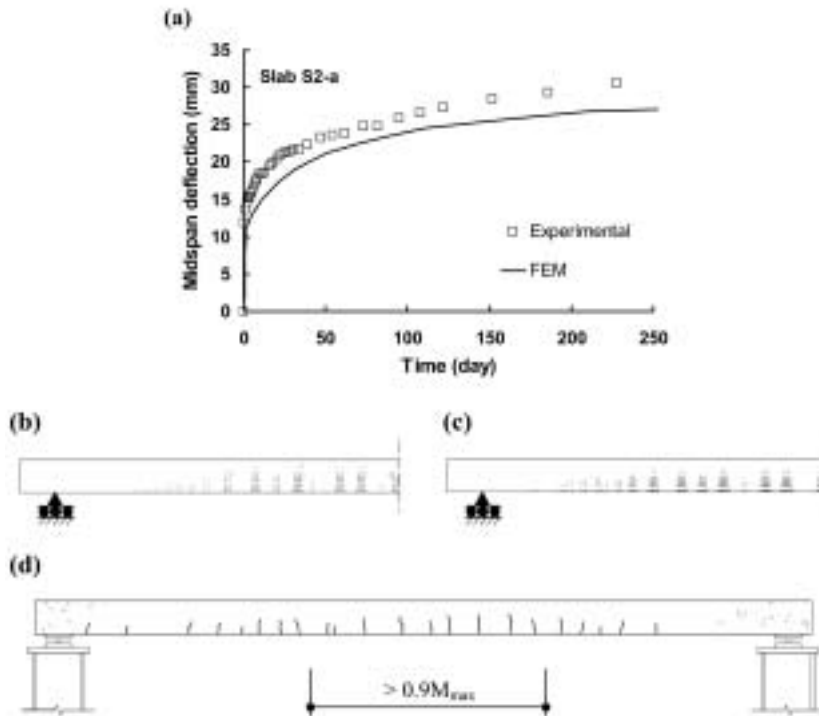


Fig. 12 Reinforced concrete slab S2-a under sustained service loads: (a) Midspan deflection versus time; (b) Instantaneous FEM crack pattern; (c) FEM crack pattern at 200 days; (d) Experimental crack pattern at 200 days

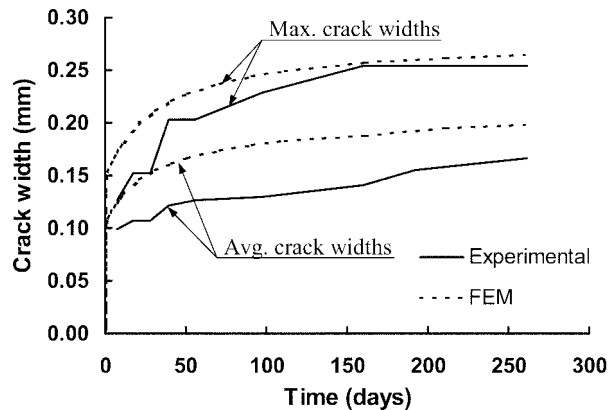


Fig. 13 Comparison of FEM and experimental crack width envelope with time for slab S2-a (for region of moment $> 0.9M_{max}$)

FE mesh used to model the slab is shown in Fig. 11c with one half of the slab modelled with symmetry. The FE model consisted of 390 nodes, 270 concrete elements and 54 steel elements. The steel and concrete were bonded via interface elements with full anchorage provided for the steel at far left end of the specimen. Slab S2-a was cast at the same time as beam B2-a, discussed above, and the material parameters and properties of the test specimen and those as given above for beam B2-a.

The midspan deflection with time for the slab specimen is shown in Fig. 12a. The finite element model slightly underestimates the time-dependent deformation but it is well within a reasonable range of calculation. The calculated crack patterns and crack width plots are shown in Figs. 12b and 12c for time at first loading and at 200 days, respectively, with an excellent agreement observed with the experimental crack pattern shown in Fig. 12e.

In Fig. 13 the crack widths calculated by the finite element model are compared with the experimental measurement for the cracks within the region of moment greater than 90% of the midspan moment (see Fig. 12d). The model calculated a slightly higher average crack opening compared to the observed test results, however, overall the agreement is reasonable with the model calculating to good accuracy the maximum crack width.

5. Conclusions

A finite element model has been presented for analysing the time-dependent behaviour of reinforced concrete members in plane stress at the serviceability limit states. The model calculates time-dependent increase in deflection and increase in crack widths. The model incorporates a bond-slip interface element between the concrete and steel elements with the calculation of localized, discrete cracks, in reinforced concrete structures made possible by introducing a bond-slip modelling technique taking account of the relative displacement between the steel and the concrete and subsequently simulating slipping at the interface. The proposed model has been shown to provide a good agreement with the observed deformation, crack distribution and crack widths for

two long-term test specimens loaded under a constant load for over 200 days.

Acknowledgements

This research was funded by Australian Research Council Discovery Grant No. DP0210039 and an Australian Government International Postgraduate Research Scholarship. The ARC and Scholarship support are gratefully acknowledged.

References

- Attard, M. M., Nguyen, D. M., and Foster, S. J. (1996), "Finite element analysis of out of plane buckling of reinforced concrete walls", *Comput. Struct.*, **61**(6), 1037-1042.
- Bazant, Z. P., and Oh, B. H. (1983), "Crack band theory for fracture of concrete", *Materials and Structures, RILEM*, **16**(93), 155-177.
- CEB-FIP (1993). Comité Euro-International du Béton Fédération International de la Précontrainte, *Model Code 1990*. Thomas Telford, London.
- Cervenka, J. (1994), "Discrete crack modeling in concrete structures", PhD Thesis, University of Colorado, Boulder.
- Darwin, D., and Pecknold, D. A. (1977), "Non-linear stress-strain law for concrete", *J. Eng. Mech. Div.*, ASCE, **103**(EM2), 229-241.
- Foster, S. J., and Marti, P. (2002), "FE modelling of RC membranes using the CMM formulation", *Proc. of the Fifth World Congress on Computational Mechanics (WCCM V), July 7-12, Vienna, Austria*, H. A Mang., F. G. Rammerstorfer, and J. Eberhardsteiner, eds., Vienna University of Technology.
- Foster, S. J., and Marti, P. (2003), "Cracked membrane model: FE implementation", *J. Struct. Eng.*, ASCE, **129**(9), 1155-1163.
- Gilbert, R. I (1988), *Time Effects in Concrete Structures*. Elsevier Science Publisher, The Netherlands.
- Gilbert, R. I., and Warner, R. F. (1978), "Tension stiffening in reinforced concrete slabs", *J. Struct. Div.*, ASCE, **104**(ST12), 1885-1900.
- Goodman, R., Taylor, R., and Brekke, T. (1968), "A model for the mechanics of rocks", *Soil Mechanics and Foundations, Division 5*, 637-659.
- Marti, P., Alvarez, M., Kaufmann, W., and Sigrist, V. (1998), "Tension chord model for structural concrete", *Structural Engineering International, IABSE*, **4/98**, 287-298.
- Mehlhorn, G., and Keuser, M. (1985), "Isoparametric contact elements for analysis of reinforced concrete structures", *Finite Element Analysis of Reinforced Concrete Structures*, C. Meyer, and H. Okamura, eds., ASCE, New York, 329-347.
- Nejadi, S., and Gilbert, R. I. (2004), "Time-dependent flexural cracking in reinforced concrete beams and slabs an experimental study", The School of Civil and Environmental Engineering, The University of New South Wales, Sydney, Australia, UNICIV Report (in preparation).
- Ngo, D., and Scordelis, A. C. (1967), "Finite element analysis of reinforced concrete beams", *ACI J.*, **64**(3), 152-163.
- Petersson, P. E. (1981), "Crack growth and development of fracture zone in plain concrete and similar materials", Report No. TVBM-1006, Division of Building Materials, Lund Institute of Technology, Lund, Sweden.
- Rots, J. G. (1985), "Bond-slip simulations using smeared crack and / or interface elements", Research Report 85-01, Structural Mechanics Group, Department of Civil Engineering, Delft University of Technology.
- Rots, J. G. (1988), "Computational modeling of concrete fracture." PhD thesis, Delft University of Technology, Delft, The Netherlands.
- Scanlon, A., and Murray, D. (1974), "Time-dependent reinforced concrete slabs deflections", *J. Struct. Div.*,

- ASCE, **100**(ST9), 1911-1924.
- Vecchio, F. J. (1989), "Nonlinear finite element analysis of reinforced concrete membranes", *ACI Struct. J.*, **86**(1), 26-35.
- Vecchio, F. J., and Collins, M. P. (1986), "The modified compression field theory for reinforced concrete elements subjected to shear", *ACI J. Proc.*, **83**(2), 219-231.

KM